JOURNAL OF MATERIALS SCIENCE **34** (1999) 5749–5756

Dynamic strains in architectural laminated glass subjected to low velocity impacts from small projectiles

R. A. BEHR*, P. A. KREMER
Department of Architectural Engineering, The Pennsylvania State University, University Park, PA 16802-1417, USA
E-mail: behr@engr.psu.edu

L. R. DHARANI, F. S. JI, N. D. KAISER
Graduate Center for Materials Research, University of Missouri-Rolla, Rolla, MO 65409-1170, USA

An experimental validation of a mechanics-based finite element model for architectural laminated glass units subjected to low velocity, two gram projectile impacts is described. The impact situation models a scenario commonly observed during severe windstorms, in which small, hard projectiles, such as roof gravel, impact windows. Controlled experiments were conducted using a calibrated air gun to propel a steel ball against simply supported rectangular laminated glass specimens. Dynamic strains on the inner glass ply were measured using foil strain gages and a high speed data acquisition system. Impact speed, interlayer thickness, glass ply thickness, and glass heat treatment conditions were varied. Dynamic strains predicted by the finite element model were in close agreement with those measured in the laboratory.

1. Introduction

Model building code procedures for the structural design of architectural glass to withstand windstorms have historically been based on the resistance of glass panels to lateral wind pressure loadings alone. However, post-storm inspections of hurricane ravaged regions have revealed that windborne debris impacts are a primary cause of ultimate failure in architectural glass during severe windstorms [1]. The failure mechanism has been documented as a sequence of windborne debris impacts followed by numerous cycles of positive and negative wind pressures, which ultimately leads to a breached building envelope [2–6]. High winds and rain entering a breached building envelope can cause extensive damage to building contents and costly disruptions of building operations. In fact, a significant portion of the damage costs associated with hurricanes has been attributed to this failure mechanism [1].

If the architectural glass is monolithic, then debris impacts that cause fracture in the glass panel will compromise its ability to sustain lateral wind pressure loadings. Laminated glass; however, which normally consists of two soda lime glass plies bonded to a thin interlayer of an elastomeric polymer called polyvinyl butyral (PVB), has shown inherent resistance to windborne debris impacts because debris impacts typically must induce fracture in both plies before the unit's ability to sustain lateral wind pressure loadings is compromised [2]. That is, the outer glass ply can be fractured, while the inner glass ply remains unfractured [6]. In this context, the outer glass ply can be considered a "sacrificial ply," because it can be fractured while the inner glass ply and the PVB interlayer remain intact. In the sacrificial ply scenario the integrity of the building envelope is preserved, provided that the inner glass ply has sufficient resistance to wind pressures for the duration of the windstorm. Another important characteristic of laminated glass is that when a glass ply fractures, fragments tend to remain bonded to the PVB interlayer and do not themselves become additional windborne debris, which mitigates the risk of personal injury and additional property damage.

To explore fully the feasibility of the sacrificial ply concept, a project to develop a design procedure for laminated glass under windborne debris impacts is currently being conducted by the authors. This new design methodology is intended to be used in conjunction with existing procedures for the structural design of architectural glass under wind pressures, such as those cited in ASTM E1300 [7]. Current work consists of developing a finite element model to evaluate the effects of low-velocity projectile impacts on laminated glass, and then validating these finite element results with appropriate laboratory tests. Laboratory validation of the analytical model is important because these analytical computations will be used extensively in developing

* Author to whom all correspondence should be addressed.

the design procedure. In addition, there is relatively little information in the literature pertaining to laboratory verifications of analytical predictions of strains and stresses in laminated glass units subjected to low velocity projectile impacts. Experimental validation of finite element analyses of windborne debris impacts on laminated glass units is the primary focus of this article.

2. Literature review

Analytical and experimental studies of projectile impacts on architectural laminated glass units have been performed [8–12]. Flocker and Dharani [9–12] modified the DYNA2D [13] finite element code to model laminated glass under simulated windborne debris impacts. Specifically, they incorporated the material properties and geometries of the glass plies and PVB interlayer, and they modeled impact effects such as outer glass ply fracturing and PVB debonding.

Although a number of publications have addressed stress wave propagation through glass and projectile impacts on glass, few publications have included experimental verifications of analytically derived stresses in glass panels under projectile impacts. Tsai and Kolsky [14] recorded strain pulses in monolithic glass specimens under projectile impacts using strain gages connected to a cathode ray oscilloscope outfitted with a wideband amplifier, and then compared these data to strains predicted by elastic half-space theory. They found that their analysis "gave surprisingly close agreement with the main pulse shapes observed experimentally." The experimental methods described later in this article are similar to those used by Tsai and Kolsky, but the analytical predictions described herein were made by applying finite element methodology, instead of using elastic half-space theory. Further, this article focuses on the impact response of laminated glass units instead of monolithic glass plates. Kajon and Steindler [15] also employed experimental procedures similar to those described herein, but they impacted locomotive windshields consisting of two plies of tempered glass, a polycarbonate ply between the two glass plies, and PVB to bond the three plies together.

Other authors [16–27] have addressed the response of glass plates to projectile impacts, wherein they reported various glass failure modes such as Hertz cone cracking, radial cracking and local crushing. Abou-el-leil *et al*. [28, 29] compared analytical and experimental stresses caused by small projectile impacts on helicopter windshields, but their analytical model was based on Hertz cone fracture theory rather than finite element analysis. Other researchers [30–32] employed finite element analyses to simulate impact loadings on glass, but the primary emphasis of these studies was to measure deflections of the glass plates or to model Hertz cone cracking.

In summary, review of the literature indicates that the scope of this article represents new work that has not been reported previously.

3. Finite element modeling

The primary purpose of this article is to validate experimentally the analytical model developed by Flocker and Dharani [9] for the analysis of windborne debris impacts on laminated glass units. A specimen matrix (Table I) of some common laminated glass configurations was selected to validate the ability of the analytical model to predict radial strains on the inner glass ply surface as a result of small projectile impacts. The experimental plan included a sufficient variety of configurations to assess radial strain response on the inner glass ply surface due to the effects of: (1) impact velocity; (2) interlayer thickness; (3) glass ply thickness; and (4) glass surface compressive prestress. The configurations in Table I were also chosen to represent a broad range of architectural laminated glass configurations found in modern building design practice.

Because details of the finite element formulation of the problem are found in Ref. [9], only a summary of the finite element model is presented in this section. A laminated glass system consisting of an outer glass ply of thickness h_o and an inner glass ply of thickness h_i adhered to a polymer interlayer (PVB) of thickness h_{PVB}, subjected to low velocity, two gram projectile impacts is shown in Fig. 1. A steel ball of radius R is included to simulate the effect of windborne debris impacts from small environmental projectiles such as roof gravel. A strain gage rosette is mounted on the exposed surface of the inner glass ply to measure the radial strain response during impacts. The point of convergence of the axes of the three strain gages in the rosette (Point A in Fig. 1) is opposite to the impact site (Point B in Fig. 1). For

TABLE I Laminated glass configurations tested under impact conditions

Laminated glass configuration	Overall specimen dimensions, H × W, mm	Total specimen thickness, mm	PVB interlayer thickness, mm	Glass ply thickness[a], mm	Surface compressive prestress, MPa (Glass type)[b]
A	305 × 305	6.72	0.76	2.98	1.8 (Both plies annealed)
B	305 × 305	10.32	0.76	4.78	4.2 (Both plies annealed)
C	305 × 305	11.14	1.52	4.81	1.7 (Both plies annealed)
D	305 × 305	11.61	2.29	4.66	2.2 (Both plies annealed)
E	305 × 305	10.94	1.52	4.71	46.6 (Both plies heat-strengthened)
F	2486 × 1473	10.78	1.52	4.63	67.1 (Both plies heat-strengthened)
G	1829 × 1524	10.96	1.52	4.72	80.6 (Both plies fully tempered)

[a]Glass ply thickness obtained by subtracting PVB interlayer thickness from total specimen thickness and dividing the result by two. Both glass plies have the same nominal thickness.

[b]Surface compressive prestress was measured with a Strainoptic Technologies, Inc. Grazing Angle Surface Polarimeter (GASP).

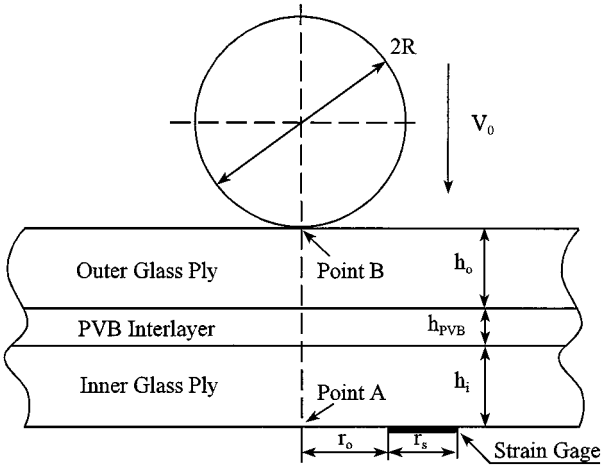

Figure 1 Schematic diagram of a laminated glass unit under a low velocity two gram steel ball impact.

the strain gage used in the experimental test, $r_o = 2$ mm and $r_s = 3$ mm in Fig. 1.

The glass plies and steel ball are modeled as linear elastic materials. The deviatoric and volumetric behaviors are given by

$$S_{ij} = \left[\frac{E\nu\epsilon_v}{(1+\nu)(1-2\nu)} + p\right]\delta_{ij} + \frac{E\epsilon_{ij}}{(1+\nu)} \quad (1)$$

$$p = -\frac{E\epsilon_v}{3(1-2\nu)} \quad (2)$$

where S_{ij} is the deviatoric stress tensor, δ_{ij} is the Kroenecker delta, ϵ_{ij} is the strain tensor, ϵ_v is the volumetric strain tensor, p is pressure, E is Young's modulus and ν is Poisson's ratio. The PVB interlayer is modeled as a linear viscoelastic material. The deviatoric stress tensor is given by

$$S_{ij}(t) = 2\int_0^t G(t-\tau)\dot{e}_{ij}(\tau)d\tau \quad (3)$$

where t denotes time, $\dot{e}_{ij}$ the deviatoric strain rate and $G(t)$ the stress relaxation modulus, which is assumed to be of the form

$$G(t) = G_\infty + (G_0 - G_\infty)e^{-\beta t} \quad (4)$$

where G_∞ is the long time shear modulus, G_0 is the short time shear modulus and β is the decay factor. The volumetric response is elastic, so the pressure p is computed from the current volumetric strain ϵ_v using

$$p = -K\epsilon_v \quad (5)$$

where K is the bulk modulus.

A nonlinear finite element code, DYNA2D [13], is employed to model the average radial strain response over the region covered by the strain gage. DYNA2D is a nonlinear, explicit, finite element code for analyzing the transient dynamic response of two-dimensional solids, and was developed by Whirley, Englemann and Hallquist at the Lawrence Livermore National Laboratory. It can be used to simulate contacts, explosives and propellants. Here, it is used to analyze the dynamic response of laminated glass units subjected to low velocity small projectile impacts. The laminated glass system and steel ball are discretized using a four-node element. A typical mesh is illustrated in Fig. 2. In the current problem, the size of the laminated glass unit is very large compared to its thickness and the size of the steel ball. It is, therefore, reasonable to assume that the radius of the laminated glass unit is infinite. To simulate this assumption in the finite element analysis, the laminated glass unit radius is limited to 40 mm, and non-reflecting boundaries are used along its perimeter. That is, no support is applied to the laminated glass unit. Under this assumption reflected stress waves do not have enough time to travel back to the center of the laminated glass unit after reaching its boundaries during the impact load duration; hence, the boundary condition of the laminated glass unit has no effect on the stress waves at its center during the impact load duration. Average radial strains at the strain gage location are computed by averaging the radial strains of the finite elements covered by the strain gage active grid. The following constants are used in the analysis [9, 33]: for glass, $E = 72$ GPa, $\nu = 0.25$, mass density $\rho = 2500$ kg/m^3; for steel, $E = 200$ GPa, $\nu = 0.29$, $R = 3.97$ mm, $\rho = 7800$ kg/m^3; and for PVB, $K = 20.0$ GPa, $G_0 = 0.33$ GPa, $G_\infty = 0.69$ MPa, $\rho = 1100$ kg/m^3 and $\beta = 12.6$ s^{-1}.

First, the effect of element size on solution convergence was investigated. Results show that average radial strain peak values decrease in magnitude and approach a constant value as element length decreases. Satisfactory convergence was achieved by limiting the element length in the radial direction to be less than or equal to 0.25 mm.

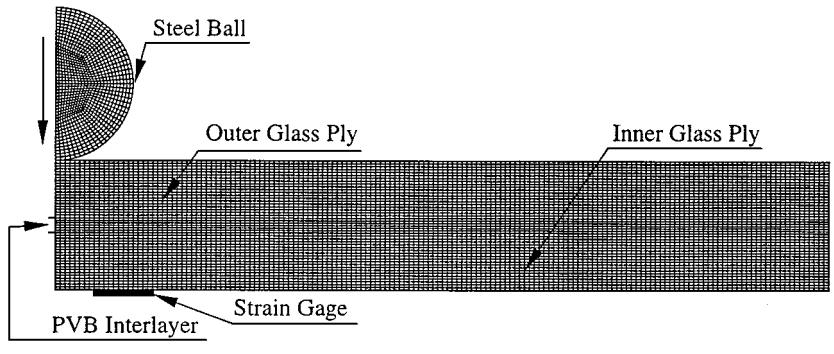

Figure 2 A typical mesh used in the finite element analysis.

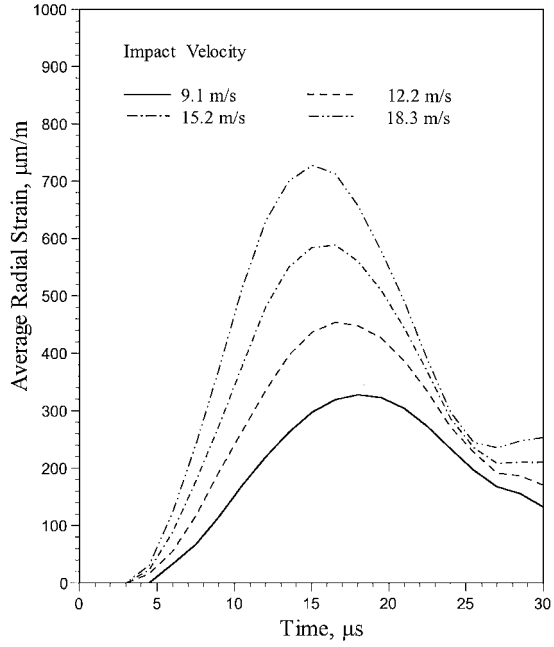

Figure 3 Typical average radial strain from finite element analysis at strain gage location for Configuration B ($h_o = h_i = 4.78$ mm, $h_{PVB} = 0.76$ mm) under a two gram steel ball impact.

Fig. 3 shows typical average radial strains at the strain gage location as a function of time after impact for various impact velocities for Configuration B in Table I. Radial strains are observed to increase monotonically with respect to increasing impact velocity. The peak of the average radial strain shown in Fig. 3 is also the peak of the entire dynamic response, since the local maximum strains generated by reflected stress waves are much smaller after the first impact pulse, which has a duration of approximately 30 μs for the impact tests performed in this study.

Effects due to variations in material properties used in the finite element analyses were also studied. Stong [34] observed a range of measured Young's modulus for glass of 71.3 to 76.2 GPa. It is found that a change in Young's modulus from 71.3 to 76.2 GPa (a 6.6% difference) produces a change in computed peak strains at the strain gage location from 316 to 303 μm/m (a 4.2% difference). With a Poisson's ratio of nearly 0.5, PVB is nearly incompressible, which implies that its bulk modulus is very large [35]. The computed peak radial strains approach a constant value as bulk modulus increases. When the bulk modulus exceeds 20 GPa, computed strains are essentially independent of bulk modulus. Thus, using a PVB bulk modulus of 20 GPa or larger in the analytical model accounts well for PVB incompressibility. The computed peak radial strains approach a constant value as the short time shear modulus G_0 decreases. When the short time shear modulus is less than 0.50 GPa, peak radial strains are approximately independent of this parameter. A short time shear modulus value of 0.33 GPa, as reported by Hwang [33], was selected for PVB in this analysis.

Initial laboratory experiments indicated that impacts with the air gun used in this study could be made consistently within 1 mm from the point of convergence of the three strain gage axes of the strain gage rosette. However, it is assumed that the point of convergence of the strain gage rosette in the finite element analysis (Point A in Fig. 1) is exactly opposite to the impact site (Point B in Fig. 1). The effects of deviation in impact location (from the point of convergence of the strain gage rosette) on the average radial strain from finite element analysis were studied. For example, with $h_i = h_o = 4.81$ mm, $h_{PVB} = 1.52$ mm and an impact velocity of 9.1 m/s, a radial impact location deviation of 1 mm from the point of convergence produces approximately 10% deviation in the peak value of the computed average strain. Thus, the effects of deviations in impact location are significant, and these effects need to be considered carefully when comparing computed finite element strains to measured strains.

In summary, a finite element approach was applied to model a laminated glass system subjected to low velocity impacts from small projectiles. Effects on the computed results due to variations in finite element size, laminated glass configuration, material properties and impact location were investigated. Computed finite element results will now be compared with corresponding experimental data for the configurations in Table I to assess the validity of the finite element model.

4. Experimental plan and test apparatus

The test apparatus in Fig. 4 was used to acquire the radial strain responses for the configurations in Table I.

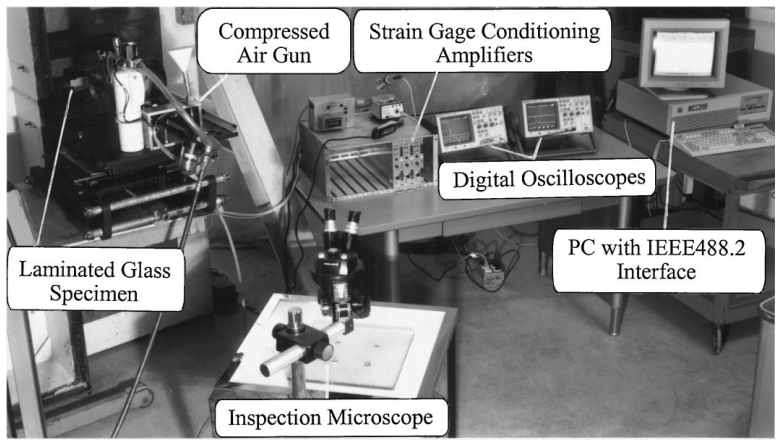

Figure 4 Test apparatus used to acquire radial strain responses for laminated glass configurations subjected to two gram steel ball impacts.

A detailed description of the test apparatus in Fig. 4 is given below.

Square, 305×305 mm laminated glass specimens as described in Table I were secured in a custom-built wooden holding frame with rubber spacers, while the larger rectangular specimens (Configurations F and G) were secured in commercially constructed aluminum frames using rubber gaskets. Thus, all specimens were simply supported along their entire perimeters. However, to be consistent with the non-reflecting boundary support condition employed in the finite element model, projectile impacts were made at sufficient distances from specimen boundaries [at least 102 mm (4 in.)] so as to minimize the possibility of wave reflection and other boundary effects in the laminated glass specimens.

A compressed air gun was fabricated in-house to propel the steel balls. Selection of the 7.94 mm diameter, 2.0 gm hardened chrome steel ball projectile was made on the basis of windstorm records and historical accounts of window glass damage caused by windborne debris impacts [36, 37]. Positioning of the air gun over the impact site was accomplished using a laser pointer as a sighting device in conjunction with a three-dimensional positioning table. All impacts were made normal to the outer glass ply with a gun muzzle-to-glass distance of 25 mm, which made velocity loss between the gun muzzle and the impact site negligible. Velocity for each impact was measured at the gun muzzle using optical sensors described by Behr and Kremer [8]. Accurate measurement of impact velocities was ensured through the use of high speed 35 mm photography under a stroboscopic light source, as well as a commercial ballistic chronograph normally used to establish muzzle velocities of firearms. Both techniques for calibrating the projectile velocities are detailed by Behr and Kremer [8]. Analysis of the recorded velocity data for all impacts made in this study indicated that impact velocity could be controlled to within ± 0.5 m/s.

Impacts were made on the outer glass ply directly opposite the point of convergence of the strain gage rosettes mounted on the exposed surface of the inner glass ply. Thus, it was necessary to transpose the location of the point of convergence to the impact side (i.e., the outer glass ply) using an inspection microscope to minimize impact location errors. Post-impact inspections indicated that each impact location could be controlled to within a radial distance of 1.0 mm from the center of the point of convergence target.

Although it is possible to fracture both glass plies of a laminated glass unit as a result of a projectile impact on the outer glass ply, fracture of the inner glass ply at the active grid location of a strain gage could lead to gage lift-off and erroneous output from that strain gage. Also, the overriding objective of the sacrificial ply design concept is to ensure that the inner glass ply of a laminated glass unit remains unfractured as a result of windborne debris impacts. For these reasons, impact velocities in this study were kept below those that would consistently cause inner glass ply fracture. The lower bound of impact velocity for each configuration was selected on the basis of laboratory trials to be 9.1 m/s (30 ft/s).

For the velocities and laminated glass configurations employed in this study, the portion of the radial strain response of most interest occurs within approximately 30 μs after impact and is characterized by a steep strain gradient. For these reasons, the data acquisition system needed to have a sufficiently high frequency response bandwidth and a sufficiently high data acquisition rate to capture the radial strain response adequately. Radial strains were measured with Measurements Group CEA-06-125UR-350 45° strain gage rosettes mounted on the inner glass ply of the specimens. Rosettes included three 350 Ω, 3.175 mm gage length constantan foil strain gages encapsulated in a polyimide backing.

Strain gage rosettes were bonded to the inner glass ply of the laminated glass specimens using Measurements Group M-Bond 200 cyanoacrylate adhesive. Light abrasion of the inner glass ply surface with a 220 grit silicon carbide sandpaper over the area to be covered by the rosette was performed to ensure good adhesion of the strain gage rosette to the glass. It is important to emphasize that the overall objective of the sacrificial ply concept is to allow the outer ply of a laminated glass unit to fracture under windborne debris impacts, but to protect against inner glass ply fracture. Thus, the strain gage measurements were intended to be made on an unfractured inner glass ply. The small amount of surface abrasion employed in this study to improve bonding of strain gages to the inner glass ply of laminated glass test specimens did not undermine the objectives of this paper, since these objectives did not include an investigation of inner glass ply failure modes as a result of projectile impacts on the outer glass ply.

Each strain gage was connected to a Measurements Group Model 2311 strain gage conditioning amplifier in a three-wire quarter bridge configuration to measure tensile strains. Conditioning amplifiers were operated in "wideband mode" to allow unfiltered passage of the strain gage signals and to maximize the frequency response of the amplifiers. Using the portion of the strain response of interest to this study as a guide (Fig. 3) indicated that the frequency component of the main strain peaks was about 33 kHz. The manufacturer's reported frequency response for the 2311 amplifiers is given as dc to 50 kHz at -0.5 dB and dc to 135 kHz at -3 dB in the wideband mode within an amplifier gain range of 100 to 1100 [38]. Additionally, the manufacturer reported that the slew rate of the 2311 amplifier is greater than 6 V/μs over all gain settings [39]. Therefore, the frequency response of the amplifiers was more than adequate for capturing that portion of the radial strain response of primary interest in this study.

Shunt calibration of the strain gage conditioning amplifiers was performed with a Measurements Group Model 1550A strain indicator calibration box. A 5 volt bridge excitation and an amplifier gain setting of 1100 on each strain gage conditioning amplifier was found to provide high signal-to-noise ratio and negligible zero shift with time. Conditioned and amplified output from the conditioning amplifiers was sent to two HP54600A, 100 MHz, two-channel digital oscilloscopes. Digitized radial strain response curves from the oscilloscopes were transferred across an IEEE488.2 interface with the

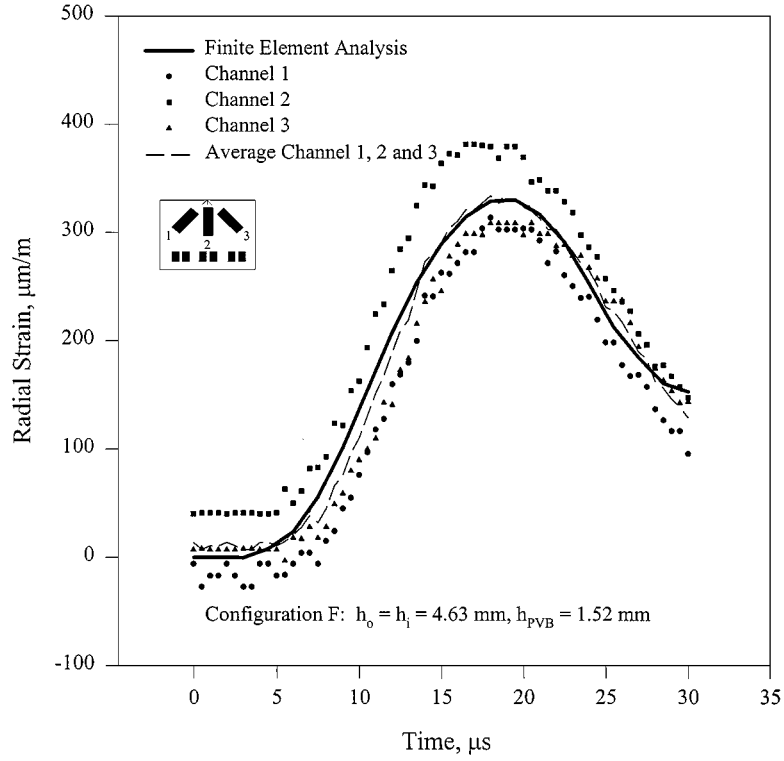

Figure 5 Representative set of radial strain response curves for each gage of one rosette during a 9.1 m/s impact on Configuration F: $h_o = h_i = 4.63$ mm, $h_{PVB} = 1.52$ mm.

aid of a program written in QuickBASIC on a 80386 personal computer for later viewing and analysis. The effective data acquisition rate was 2.0 million samples per strain gage channel per second (2.0 MHz), which permitted the strain pulse from each strain gage to be captured and graphed with precision. At a data acquisition rate of 2 MHz, approximately 0.5 μs elapses between samples. For a strain pulse with a duration of 30 μs, approximately 30 μs $\div$ 0.5 μs/point = 60 points are available to plot the main portion of the strain pulses presented in this article (Fig. 5).

5. Results and discussion

It is important that finite element strain computations and experimental strain measurements for each configuration be put on the same basis in order to ensure rational comparisons between the two sets of results. Average peak strains from the finite element analysis were computed over the region covered by the active grid of each strain gage, because strain gage measurements represent an average strain over the active grid of the gage. In addition, because the middle gage of each rosette was 1.27 mm closer to the point of convergence of all three gages as compared to the other two gages, it was necessary to account for this position variance in the finite element model computations.

A representative set of radial strain response curves for each gage of one rosette during a 9.1 m/s impact on Configuration F is shown in Fig. 5, along with the average radial strain response as predicted by finite element analysis. It should be noted that the curves in Fig. 5 represent only that portion of the radial strain response of interest to this study. It is clear from Fig. 5 that the measured radial strain response compares closely in both shape and magnitude with the finite element prediction. Fig. 5 also shows that the radial strain of the middle gage of the rosette (Channel 2) is higher than those in the other two gages, due to the aforementioned fact that the middle gage was 1.27 mm closer to the point of convergence of all three gages as compared to the other two gages. Measured radial strains for the middle gage were typically 15 to 20% higher than the other two gages, which was reasonable given its closer proximity to the point of impact.

Comparisons of peak radial strains from the finite element analysis to those measured experimentally are given in Table II. Variations in the number of data points (n) reported in Table II are generally due to the fact that some impact locations were impacted more than once when no visible damage was noted on the glass surface after a prior impact. Inspection of the data for those cases where multiple impacts were made on a given impact location indicated that multiple impacts had no noticeable effect on measured radial strains, provided that earlier impacts at the same location produced no visible surface damage, as detectable by the unaided eye to the outer glass ply. In a limited number of instances, data from strain gage rosettes were not used due to incomplete adhesion to the glass substrate.

Table II contains a summary of computed and measured peak strains on the inner glass ply surface for laminated glass Configurations A through G under two gram steel ball impacts. Coefficients of variation in measured peak strains range from a low of 1.5% to a high of 26.0%, with an average of 15.6% for the values reported in Table II. Percent differences between finite element and experimental peak strains in Table II

TABLE II Computed and measured peak strains on inner glass ply surface due to a two gram steel ball impact

Laminated glass configuration	Impact velocity, m/s (ft/s)	Finite element average peak strain (μm/m)[a]	Measured mean peak strain, $\pm$one standard deviation (μm/m)[a]	Percent difference (%)[b]
A	9.1 (30)	580	580 ± 130 (CV = 22.4%; $n = 16$)[c]	0.0
	12.2 (40)	780	770 ± 200 (CV = 26.0%; $n = 11$)	1.3
B	9.1 (30)	330	360 ± 50 (CV = 13.9%; $n = 13$)	8.7
	12.2 (40)	450	420 ± 80 (CV = 19.0%; $n = 6$)	6.9
	15.2 (50)	590	580 ± 130 (CV = 22.4%; $n = 6$)	1.7
	18.3 (60)	730	790 ± 70 (CV = 8.9%; $n = 6$)	7.9
C	9.1 (30)	310	260 ± 40 (CV = 15.4%; $n = 9$)	17.5
	15.2 (50)	560	630 ± 80 (CV = 12.7%; $n = 6$)	11.8
	18.3 (60)	690	650 ± 10 (CV = 1.5%; $n = 5$)	6.0
D	9.1 (30)	310	280 ± 30 (CV = 10.7%; $n = 5$)	10.2
	15.2 (50)	560	550 ± 80 (CV = 14.5%; $n = 5$)	1.8
	21.3 (70)	830	790 ± 130 (CV = 16.5%; $n = 5$)	4.9
E	9.1 (30)	320	360 ± 50 (CV = 13.9%; $n = 8$)	11.8
	21.3 (70)	840	940 ± 200 (CV = 21.3%; $n = 7$)	11.2
F	9.1 (30)	330	310 ± 30 (CV = 9.7%; $n = 12$)	6.3
	21.3 (70)	860	940 ± 240 (CV = 25.5%; $n = 8$)	8.9
G	9.1 (30)	320	310 ± 20 (CV = 6.4%; $n = 6$)	3.2
	21.3 (70)	840	1020 ± 210 (CV = 20.6%; $n = 4$)	19.4

[a]Peak strains are rounded to the nearest 10 μm/m.
[b]Percent difference between finite element and measured peak strains is calculated as follows: $\left| \frac{\text{finite element} - \text{measured}}{(\text{finite element} + \text{measured}) \div 2} \right| \times 100\%$.
[c]CV = coefficient of variation [(standard deviation $\div$ mean) $\times$ 100%]; $n =$ number of data points.

range from 0 to 19.4%, with an average of 7.7%. Thus, the experimental strain data are repeatable, and the correlations between finite element predictions and experimental data are good.

When comparing Configurations B, C and D in Table II (i.e., Configurations B, C, and D have the same nominal glass ply thickness, but have different PVB interlayer thicknesses), a slight decrease in peak radial strain is observed as PVB interlayer thickness increases in both the finite element analysis results and the laboratory measurements. Glass ply thickness appears to have a more pronounced effect on peak radial strains, as seen when comparing peak strains at the same impact velocity for Configurations A and B in Table II (i.e., Configurations A and B have the same PVB interlayer thickness but have different nominal glass ply thicknesses).

Surface compressive prestress, as present in heat-strengthened and fully tempered glass types, had no apparent effect on measured peak strrains caused by projectile impacts, as seen when comparing peak strains at the same impact velocity for Configurations C, E, F and G in Table II (Configurations C, E, F and G all have the same nominal glass ply thicknesses and PVB interlayer thickness, but the glass plies are comprised of different glass types). This would be expected, since the stresses due to the impact loading are superimposed on the surface compressive prestresses that pre-exist in heat-strengthened and fully tempered glass plies. Since strain gages measure strain differentials from an unloaded (unstrained) condition to a loaded (strained) condition, superimposing tensile strains to heat-strengthened and fully tempered glass surfaces causes these surface strains to become "less negative." Thus, although Table II shows no significant differences in peak strains (or, more precisely, peak strain differentials) due to projectile impacts as a function of glass type, the presence of surface compressive prestress in heat-strengthened and fully tempered glass types will

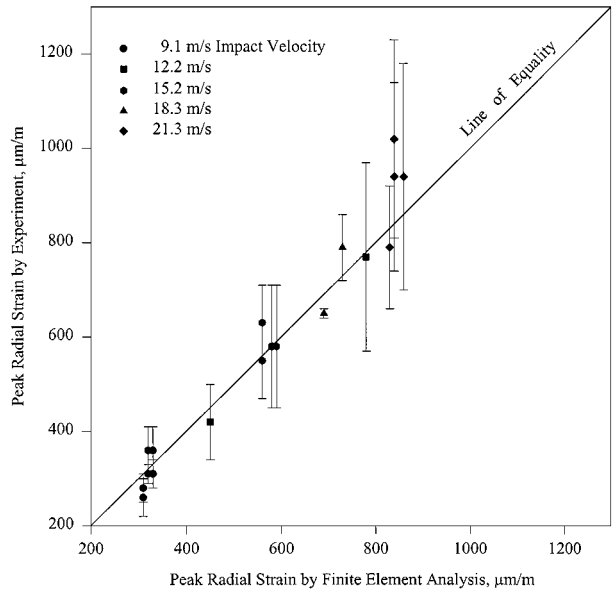

Figure 6 Peak radial strains by finite element analysis and by experiment on inner glass ply surface of all laminated glass configurations tested under a two gram steel ball impact.

increase the overall fracture resistance of inner glass plies under windborne debris impacts, as reported earlier by Behr and Kremer [8]. Improved impact resistance can be expected from heat-strengthened and fully tempered glass types because one mode of glass fracture is related to the net tensile stress on a given glass surface.

A graphical summary of all computed and measured peak strains in this test program is given in Fig. 6. Distribution of data about the 45° line of equality in Fig. 6 demonstrates the close overall correlation between the finite element computations and the measured strain data. It is also interesting to note that this close correlation between the finite element computations and the measured strain data exists despite the fact that damage to the outer glass ply was not explicitly incorporated

into the finite element computations. Thus, for this impact scenario, it does not appear important in the finite element formulation to model outer glass ply damage in order to calculate reasonably accurate inner glass ply strains.

6. Conclusion

This study confirmed the ability of an analytical finite element model to predict accurately the peak strains in representative architectural laminated glass units as functions of impact velocity, laminate configuration, and component material properties. Correlations between peak radial strains computed using finite element analysis and those measured experimentally were close, with the average difference between analytical predictions and experimental data being 7.7%. Peak radial strain increases significantly as projectile impact velocity is increased, and peak radial strain decreases significantly as glass ply thickness is increased. Peak radial strain decreases only slightly, however, as PVB thickness is increased, and peak radial strain (or, more precisely, the increment of peak radial strain due to projectile impact) is unaffected by the existence of a state of compressive prestress on the glass surface—as exists in heat-strengthened and fully tempered glass. Thus, net glass surface stresses due to heat treatment during manufacture and projectile impacts during service can be obtained by straightforward algebraic superposition of these stresses.

The successful experimental validations of finite element computations performed in this study accomplished an important step toward developing a comprehensive, mechanics-based, failure prediction model for laminated glass units under low velocity projectile impacts such as those encountered during severe windstorms. Specifically, strains and stresses computed by finite element analysis will be related to the probability of inner glass ply failure in laminated glass units under windborne debris impacts. Then, a design procedure will be developed for architectural laminated glass units wherein only the outer (exterior) glass ply is broken during windborne debris impacts. Provided that the unbroken inner glass ply is designed for the appropriate lateral wind pressures, the resulting "sacrificial ply" laminated glass units will improve significantly the overall resistance of building envelope systems to the ravaging effects of severe windstorms.

Acknowledgements

This work is being supported by the U.S. National Science Foundation, the Missouri Department of Economic Development through the Manufacturing Research and Training Center, the E.I. duPont de Nemours and Company, and Solutia, Inc.

References

1. P. R. SPARKS and S. A. BHINDERWALA, in Hurricanes of 1992, Proceedings of ASCE Symposium, Miami, FL, December 1–3, 1993 (ASCE, New York, 1994) p. 111.
2. Anonymous, *Glass Dig.* **74**(2) (1995) 47.
3. P. E. BEERS, *Prog. Archit.* **74**(9) (1993) 76.
4. Anonymous, *Eng. News Rec.* **211**(8) (1983) 10.
5. Anonymous, ASTM *Standardization News* **21**(12) (1993) 13.
6. W. L. BEASON, G. E. MEYERS and R. W. JAMES, *J. Struct. Eng.* **110**(12) (1984) 2843.
7. ASTM E1300-97, "Standard Practice for Determining Load Resistance of Glass in Buildings" (American Society for Testing and Materials, Philadelphia, PA, 1997).
8. R. A. BEHR and P. A. KREMER, *J. Archit. Eng.* **2**(3) (1996) 95.
9. F. W. FLOCKER and L. R. DHARANI, *Eng. Struct.* **19**(10) (1997) 851.
10. *Idem., J. Mater. Sci.* **32** (1997) 2587.
11. *Idem.*, accepted for publication, *Struct. Eng. Mech.* **6**(2) (accepted for publication).
12. *Idem., J. Archit. Eng.* **4**(1) (1998) 12.
13. R. G. WHIRLEY, B. E. ENGLEMANN and J. O. HALLQUIST, "DYNA2D, a Nonlinear, Explicit, Two-Dimensional Finite Element Code for Solid Mechanics," User Manual, Lawrence Livermore National Laboratory Report UCRL-MA-110630, 1992.
14. Y. M. TSAI and H. KOLSKY, *J. Mech. Phys. Solids* **15** (1967) 263.
15. G. KAJON and R. STEINDLER, *Exp. Tech.* **21**(3) (1997) 23.
16. R. AKCAKAYA and J. R. VARNER, *Glastech. Ber.* **64**(10) (1991) 261.
17. A. BALL and H. W. MCKENZIE, *J. Phys. IV* **4**(8) (1994) C8-783.
18. A. BALL, *Philosophical Magazine A* **73**(4) (1996) 1093.
19. *Idem., J. Phys. IV* **7**(3) (1997) C3-921.
20. M. M. CHAUDHRI and C. R. KURKJIAN, *J. Amer. Ceram. Soc.* **69**(5) (1986) 404.
21. M. M. CHAUDHRI and C. LIANGYI, *Nature* **320**(6) (1986) 48.
22. M. M. CHAUDHRI and S. M. WALLEY, *Philos. Mag. A* **37**(2) (1978) 153.
23. R. J. HAND and J. E. FIELD, *Eng. Fract. Mech.* **37**(2) (1990) 293.
24. R. N. HAWARD, *J. Soc. Glass Technol.* **28** (1944) 5.
25. H. P. KIRCHNER and R. M. GRUVER, *Mater. Sci. Eng.* **28** (1977) 153.
26. C. G. KNIGHT, M. V. SWAIN and M. M. CHAUDHRI, *J. Mater. Sci.* **12** (1977) 1573.
27. W. P. SCHONBERG, *J. Spacecr.* **28**(1) (1990) 118.
28. M. M. ABOU-EL-LEIL, F. A. CAMARATTA and R. R. DIGENOVA, *Fract. Mech. Ceram.* **7** (1986) 197.
29. *Idem., J. Amer. Ceram. Soc.* **69**(9) (1986) 713.
30. W. F. ADLER and D. J. MIHORA, *Proc. SPIE-Int. Soc. Opt. Eng.* **2286** (1994) 264.
31. S. Y. CHEN, T. N. FARRIS and S. CHANDRASEKAR, *Int. J. Solids Struct.* **32**(3/4) (1995) 329.
32. C. SRIDHAR and K. P. RAO, *Comput. Struct.* **54**(6) (1995) 1183.
33. C. R. HWANG, "Computer Aided Analysis of the Stress/Strain Response of High Polymers," 2nd ed. (Technomic Publising Company, Lancaster, PA, 1994).
34. G. E. STONG, *J. Amer. Ceram. Soc.* **20** (1937) 16–22.
35. Monsanto Chemical Company, "Saflex^{TM} Polyvinyl Butyral Interlayer Laminating Guide," (Monsanto Chemical Company, St. Louis, MO, 1991).
36. R. A. BEHR, J. E. MINOR and P. A. KREMER, "Effects of Accelerated Weathering on Architectural Laminated Glass in a Windstorm Environment," in Science and Technology of Building Seals, Sealants, Glazing, and Waterproofing Vol. 6: ASTM STP 1286, Edited by J. C. Myers (American Society for Testing and Materials, Philadelphia, PA, 1996) p. 1253.
37. C. P. PANTELIDES, A. D. HORST and J. E. MINOR, *J. Struct. Eng.* **119**(2) (1993) 454.
38. Measurements Group Incorporated, "Bulletin 251: 2300 System Signal Conditioning Amplifier," (Measurements Group, Raleigh, NC, 1985).
39. Discussion with Measurements Group Technical Support, November 20, 1996.

Received 25 November 1998
and accepted 23 June 1999